Contents — P through Z

APPLICATION OF GRAVITY DATA TO UNDERSTANDING IMPACT MECHANICS. J. B. Plescia, U. S. Geological Survey, 2255 N. Gemini Drive, Flagstaff AZ 86001, jplescia@usgs.gov..

Introduction: Gravity data provide important constraints on morphometry of impact structures and on the crustal response to the impact process [1-3]. Such data can provide insight that may not be obtainable from surface geologic mapping and may not be quickly or cheaply obtained by other geophysical means. The gravity data can be used to constrain the dimensions of a completely to partly buried structure (e.g., diameter, central uplift, etc.) and can provide information on the subsurface character of both exposed and buried structures. Gravity data can also be used to reject some structures as being of impact origin.

Morphometry: The most direct use of gravity data is establish morphometric properties of partly to completely buried structures. Gravity data have been used at several structures in Australia to establish the nature of these impacts. Mulkarra was proposed [4] to be a 9 km diameter simple crater in a sedimentary section. Gravity data [5], however, reveal positive and negative anomalies that indicate the structure is actually an 18-20 km complex structure with an 8 km central peak or peak ring. At Kelly West [6], gravity data have been used to study the central uplift area. Those data (a low surrounded by a high associated with the central uplift) suggest the central uplift is a small central peak-ring filled with breccia rather than a solid central peak. At the Manson impact [7] gravity data show that the central uplift is probably an incipient peak ring and that the zone of low density material (breccia) extends to a depth of 3 km.

Deep Crustal Effects: Gravity data can be used to provide constraints on the depth of crustal deformation. Impacts produce shock effects which reduce the effective density of rocks at depths greater than the transient cavity filled with the breccia lens. At Meteor Crater the breccia lens is 220 m thick, yet the zone of low density persists to a depth of 800 m [8]. Shock waves from the impact event had sufficient energy to significantly fracture the basement for distances of 500-600 m below the crater floor, thus providing a constraint on the energy decay rate. The breccia and the shattered basement contribute to the total 0.6 mGal anomaly [9].

Upheaval Dome is a deeply eroded complex crater in Utah [10], although apparently not everyone agrees with this interpretation [11]. Detailed geologic mapping show that the normal faults that are exposed around the margin of the structure and which cut the Navajo, Kayenta and Wingate units flatten at depth. From the attitudes of the exposed faults, the faults probably flatten into a decollement within the deeper Cutler Group. Such a geometry would imply that the deformation was restricted to levels above the Culter. Gravity data collected over the structure show that there is no gravity anomaly. The absence of an anomaly is explained in that at the current structural level deformation is entirely associated with slip along faults translating different sandstone blocks. Simple translation does not produce a density contrast. Erosion is at such a level that the breccia lens has been removed. These data indicate the shock did not have substantial influence below the level of the decollement.

The gravity data for an impact structure can also be used to model the nature of the central uplift. The Connolly structure in Australia [12] is a 9 km diameter complex crater. Gravity data reveal the presence of a high over the central uplift surrounded by an annular lower amplitude high over the crater interior. The central gravity high is due to uplift of deeper sandstones from a depth of ~1 km. These sandstone are of higher density than the surrounding rock and have shed relatively high density material into the crater interior causing the annular high.

Summary: These examples serve to illustrate that gravity can provide information on the deep structure of impacts. Such data place constraints on the cratering process by providing insight into how the crust responds to the impact: how deep the effects of the shock extend, how much structural uplift occurs, the shape of the central uplift with depth, etc.

References: [1] Grieve, R. A. F., and Pilkington, M. (1996) AGSO J., 16, 399-420. [2] Pilkington, M. and Grieve, R. A. F. (1992) Rev. Geophys., 30, 161-181. [3] Plado, J. et al. (1999) GSA Special Paper 229-239. [4] Flynn, M. (1989) The Cooper and Eromanga Basins Australia, 431-439. [5] Plescia, J. B. (1999) *Berichte zur Polarforschung, 343*, 74-78. [6] Shoemaker, E. M. and Shoemaker, C. S. (1996) *AGSO J.*, 16, 379-398. [7] Plescia, J. B. (1996) *GSA Special Paper 302*, 89-104. [8] Ackerman, H. D., et al. (1975) *JGR, 80*, 765-775. [9] Regan, R. D. and Hinze, W. J. (1975) *JGR, 80*, 776-788. [10] Kriens B. J. et al. (1999) *JGR, 104*, 18867-18887. [11] Jackson, M. P. A. et al. (1998) *GSA Bull., 110*, 1547-1573. [12] Shoemaker, E. M. et al. (1989) LPSC 20th, 1010-1011.

IMPORTANCE OF TARGET PROPERTIES ON PLANETARY IMPACT CRATERS, BOTH SIMPLE AND COMPLEX. P.M. Schenk, Lunar and Planetary Institute, Houston TX 77058 (schenk@lpi.usra.edu)

Introduction: For 20 years, the issue of whether surface gravity or target properties control the shape of planetary craters has continued unabated. Periodic revisions to and questions about quality control of the planetary crater database have vexed the debate. Here I review the current status of the observations and our understanding of the results. The observational data fall into two related categories: crater depths, and morphologic transitions from one landform to another. As it turns out there is more than one way to measure these transitions. It would appear that both target gravity and properties are important.

Silicate Planets: Pike [1] made one of the first attempts to compare crater morphology on the silicate terrestrial planets, using data from the Moon, Mars and Mercury. The effort to sort out the relative importance of surface gravity and target properties (i.e., crustal strength) is complicated by the small number of such bodies for which we have data (5) and the influence of other forces. Three of these bodies (Earth, Venus, and Mars) have substantial atmospheres, which may couple to the ejecta curtain and alter landforms [2]. Earth and Mars have been subject to substantial surface erosion and modification, and crater data for Earth, which together with Venus represent the high-gravity end of the spectrum, is wholly unreliable. Magellan stereo allows depth measurements to be made [3] but the dense atmosphere prevents the formation of simple craters (by assuming lunar-like simple crater morphology, an estimate of transition diameters can be made).

Although there is clearly a general inverse trend of transition diameters with gravity from the Moon to the other higher-gravity bodies, the result of these competing forces is something akin to confusion. There appear to be major differences in morphology on Mercury and Mars, where surface gravity is otherwise similar. Pike [1] reports significant differences in the depths and transition diameters of craters on the lunar mare and on the highlands. This points to an important role for material properties, with the regolith rich highlands have a different strength than the less heavily cratered basaltic mare. Additional evidence for or against the influence of layering or rock type will be reviewed, including the latest MGS results.

Icy Satellites: The icy satellites of the outer planets are a different ball of ice. There are at least a dozen such moons for which we have data and which have complex craters. They are also of sufficiently different size that a large gravity range can be examined. Chapman and McKinnon [4] and Schenk [5] made the first satellites comparisons, suggesting that in fact there was a strong dependence of complex crater depths and transition diameters on surface gravity, but also, that these were significantly smaller than would be expected from comparison with silicate-rich planets. These observations were based on Voyager data, but subsequent Galileo data has shown that the Ganymede data was partially compromised by resolution insufficient to resolve simple craters. Callisto and Europa have also been added. The updated transitions and depths [6] clearly show that the icy satellites all fall on a g^{-1} trend. The only exceptions are Enceladus and Mimas. Enceladus craters are very irregular even by icy satellite standards and it is likely that these craters have been modified, possibly by volcanism [7]. Mimas remains to be explained, but unusually low internal porosity conditions may or may not be involved.

The unusual complex crater landforms on the larger icy satellites, especially Europa, may point to the importance of thin lithospheres and possibly liquid layers at shallow depths [6,8]. These morphologies and their dimensions provide key constraints that can be used to model icy satellite interiors [9].

Future Shock: On silicate bodies, additional data at the low end of the gravity spectrum is needed. All asteroids observed to date are too small to allow complex crater formation. The Dawn mission to Vesta and Ceres will be important for adding rocky bodies of low to moderate gravity to the data set, and indeed I will venture a prediction as to transition diameters on these bodies. Until then, the case of the silicate planets remains uncertain. For the icy satellites, a better understanding of the internal structure of Mimas is required. We might see something unexpected on two-faced Iapetus. There is also some scatter in the small saturnian satellite data which could use clearing up. Mapping of crater morphology on Titan, similar in size to Ganymede and Callisto, will be useful for comparison, although the atmosphere there may cloud the issue. Cassini beginning in 2004 should address these needs. It is curious that we do not see substantial differences between those satellites believed to be mostly water ice, and those with more exotic (and lower strength) ices such as ammonia, carbon dioxide and nitrogen (e.g., Ariel, Miranda and Triton). Pluto and other Kuiper Belt objects may be much richer in these ices and could behave differently. We have only a decade to wait (hopefully)!

References: [1] Pike, R., *Icarus*, 43, 1 (1980). [2] Schultz, P., *J. Geophys. Res.*, 97, 16183 (1992). [3] Herrick, R., & B. Sharpton, *J. Geophys. Res.*, 105, 20245 (2000). [4] Chapman, C., & W. McKinnon, in *Satellites*, U.of A. Press (1986). [5] Schenk, P., *J. Geophys. Res.*, 96, 15635 (1991). [6] Schenk, P., Nature, 417, 419 (2002). [7] Schenk, P., & J. Moore. *J. Geophys. Res.*, 100,19009 (1995). [8] Moore,J., et al., *Icarus*, 135, 127 (1998). [9] Turtle, E., & B. Ivanov, LPSC XXXIII, (abst. 1431, 2002).

IMPACT CRATER MORPHOLOGY AS A GUIDE TO REGOLITH STRUCTURE AT TAURUS-LITTROW. H. H. Schmitt[1], [1]University of Wisconsin-Madison, P.O. Box 90730, Albuquerque, NM 87199, schmitt@engr.wisc.edu.

Introduction: Mapping of variables in primary crater morphology relative to crater size can be used as an initial guide to factors that will affect mining and processing of that material for lunar resources such as helium-3, hydrogen, oxygen and water. Although time did not permit the systematic mapping of craters during the Apollo 17 exploration of the Valley of Taurus Littrow, the writer was able to provide descriptions of the variety of crater morphologies present (1).

About 3.5 b.y. ago (2), the Valley of Taurus-Littrow and its surroundings had been blanketed with a dark, pyroclastic mantle (3,4). Orange and black varieties of this mantle were specifically sampled at Station 4, Shorty Crater (5) as well as being a significant component of most samples of the regolith (4). All of the craters investigated, observed, and described are younger than the period of pyroclastic mantling. Every later impact, however, re-mobilized the fine pyroclastic material as well as the developing regolith, partially mantling all nearby younger materials.

Crater Age: The primary process that visibly ages impact craters on the Moon is the impact of small and micro-meteors over time (6) and the associated deposition of nanophase iron on all particle surfaces (7). Micro-meteor impacts generally keep the surfaces of boulders clear of this debris.

Small-scale impact processing of the upper few centimeters of the lunar surface gradually degrades and/or buries the primary features of larger impact craters and their ejecta. Crater age Category One (C1) are ubiquitous in Taurus-Littrow [<1 m.y.?]. They consist of the youngest and statistically the smallest craters and are characterized by bright halos and irregular but coherent pools of impact glass on their floors and regolith breccia fragments scattered on their walls, rims and ejecta blankets. Category Two (C2) craters include several observed on the traverse from Challenger to Station 2 and Van Serg Crater at Station 9 [1.5-3.7 m.y. (8,9)]. Relative to C1 craters, the bright halo has faded in C2 craters. Category Three (C3) craters, such as Ballet Crater [2-5 m.y. (8,10)], the coherent masses of impact glass have disappeared but fragments of regolith breccia have been retained. Category Four (C4) craters, including Shorty Crater at Station 4 [10-19 m.y. (4,11)], are marked by the full degradation of visible regolith breccia fragments. If a C4 crater is large enough to have penetrated to bedrock, it will have visible bedrock fragments on their floors and in their walls and ejecta blankets.

Additional age categories can be defined for craters large enough to expose bedrock in their floors and/or have bedrock as part of their ejecta blankets. Category Five (C5) craters have no visible bedrock on their floors even though bedrock fragments are exposed in the walls and in their ejecta blankets. Examples of C5 craters are Camelot Crater at Station 5 [70-95 m.y. (4)], Emory Crater at Station 1 [~100 m.y. (12)]. Category Six (C6) craters, such as Horatio Crater, have bedrock fragments exposed only in their walls.

Regolith Depth: Fresh craters that penetrate the regolith have fragments of the underlying bedrock on their rims as well as exposing that bedrock on their floors. They can be used to map variations in the depth of the regolith.

Regolith Layering: Craters with continuous interior benches in their walls give an indication of a significant discontinuity in the physical properties of the regolith with depth. Generally, as apparently is the case with Van Serg Crater, a bench indicates a sharp increase in compaction or strength with depth. An extreme version of a bench crater, given the field name of "pit bottomed crater," may indicate a sharp decrease in compaction or strength with depth. Pit bottomed craters were only observed on the light mantle and may indicate better compaction near the top of the light mantle than lower down as might be expected in a fluidized avalanche deposit (5).

Buried Boulder Concentrations: Craters of insufficient size to penetrate the regolith to bedrock, but which have boulders in their ejecta blankets are indicative of a concentration of buried boulders, presumably ejecta from a larger crater. Radar scans, including look-ahead radar from a mining-processing machine, might be employed to fully map a buried boulder field.

References: (1) Schmitt, H. H., (1972) in E. Jones, (2002) Apollo Lunar Surface Journal: http://www.hq. nasa.gov/ office/pao/History/alsj/ frame.html; (2) Tera, F., and G. J. Wasserberg (1976) Lun. Sci. VII Absts., LSI, 858-860; (3) Lucchitta, B. K. (1973) Lun. Sci. Conf. 4, **1**, Geochim. Cosmochim. Acta, Supp. 6, 149-162; (4) Wolfe, E. W., et al. (1981) The Geologic Investigation of the Taurus-Littrow Valley: Apollo 17 Landing Site, Geol. Sur. Prof. Paper 1080, 96-98; (5) Schmitt, H. H. (1973) Science, **182**, 687-688; (6) Shoemaker, E.M. (1968) Surveyor Project Final Rept., Part II, JPL Tech. Rept. 32-1265, NASA SP-146, 21-136; (7) Taylor, L. A. et al. (2001) J. Geophys. Res. (Paper 2000JE0011402), 27,985-27,999; (8) Yokoyama, Y., et al. (1976) Lun. Sci. Conf. 7 Absts., LSI, 956-958; (9) Bhandari, N., et al. (1976) Lur. Sci. Conf. 7 Absts., LSI, 49-51; (10) Corzaz, G., et al, (1974) Lun. Sci. Conf. 5, Geochim. et Cosmochim. Acta, Supp. 5, 2475-2499; (11) Eugster, O., (1977) Lun. Sci. Conf. 3 Absts., LSI, 3059-3082; (12) Arvidson, R., (1976) Lun. Sci. Conf. 7, **3**, Geochim. Cosmochim. Acta, Supp. 7, 2817-2832

ATMOSPHERIC EFFECTS AND OBLIQUE IMPACTS: COMPARING LABORATORY EXPERIMENTS WITH PLANETARY OBSERVATIONS. Peter H. Schultz, Brown University, Department of Geological Sciences, P. O. Box 1846, Providence, RI 02912, peter_schultz@brown.edu

Introduction: Without direct observations of a major impact, one of the few ways to study the impact process is by assessing the effects of its environment (gravity, atmosphere) or conditions of impact (e.g., impact angle). The purpose of this contribution is to review selected consequences of both the atmosphere and impact angle as witnessed in laboratory experiments or revealed by large-scale craters preserved on different planets.

Atmospheric Effects: The lunar impact cratering record is an invaluable template for interpreting the pristine cratering record on other planets. In addition to its lower gravity, the absence of an atmosphere simplifies the cratering process. While it is often assumed that the tenuous atmosphere of Mars is overwhelmed by both the initial blast and the later advancing ejecta curtain, this assumption can be shown to be unwarranted. The atmosphere does play a significant role in modifying the late-stage ejecta emplacement but this role changes as a function of target, scale, and atmospheric pressure/density. The challenge is to identify meaningful tests to isolate this effect from other processes whether through statistical studies of the planetary cratering record or by case studies.

Laboratory impact experiments provide fundamental clues for assessing atmospheric effects since the process is complex and evolving. Such experiments are not just one-to-one comparisons between results in the laboratory and examples on the planets. Rather they should be designed to isolate variables in order to enable appropriate extrapolations. For example, performing an impact experiment at 100 bars to reproduce conditions on Venus or 6mbars to simulate conditions on Mars would only produce a crater of that particular size, in that specific target. Such laboratory observations combined with theory have yielded important predictions that can be tested by the planetary impact record. Applications to Mars and Venus illustrate this strategy which elevate the discussion beyond "look-alike" comparisons.

The distinctive ejecta facies surrounding craters on Mars have generated a range of interpretations. The fluidized appearance has commonly been used to interpret the presence of buried water (1, 2). Although popular ("follow the water" theme), this could be the planetary equivalent of a mirage. It is valid to assume explicitly that fluidized ejecta represents the presence of water and then explore the implications of this extrapolation; it is not valid, however, to simply state that fluidized ejecta deposits provide evidence for water. The problem is more ambiguous….and much more interesting.

Extensive laboratory impact experiments demonstrated that the response of the atmosphere to the crater formation is as important as the effect of the atmosphere on the ejecta. Early studies noted that the atmospheric drag acting on individual ejecta should be profound, even on Mars (3). For a given crater size (hence ejection velocity at the same stage of crater growth), atmospheric drag arrests the ballistic range over a relatively narrow size range of the ejecta (factor of 10) when scaled to the ambient atmospheric density. Conversely, for a given atmospheric density and ejecta size, the effect of drag increases with increasing crater size. If blindly applied, such considerations predict that ejecta would never get out of the crater for very fine-grained ejecta (25 microns in laboratory experiments and centimeter sizes for 10 km-diameter crater on Mars). But both experiments and the existence of excavated craters on Mars (not to mention Venus) demonstrate that craters do form. The paradox was resolved by recognizing that kinematic flow created by the outward moving ejecta curtain set up intense vortices that entrain sufficiently small decelerated ejecta (4, 5). Moreover, the presence of even a small fraction (10% by weight) of such a fine-grained component can change ballistically ejected material into a vortex with tornadic velocities. Then by isolating the controlling variables, later studies were able to compare models of the kinematic flow field with simplified experiments using controlled conditions in a wind tunnel (6, 7).

Such comparisons between models and observations both in the laboratory and on planetary surfaces led to specific predictions for ejecta deposits on Mars (4, 5, 8). First, onset for fluidized ejecta should depend on crater size due to the combination of increased ejection velocities and decreased ejecta sizes (comminution). Second, run-out distances scaled to crater radius should be proportional to crater size on Mars due to increasing ejecta entrainment (but decrease on Venus). Third, increased run-out distances with increasing latitude reflect an increased fraction of fine-grained sediments. Fourth, rampart-terminated ejecta facies represent coarser grained fractions that were mobilized but not fully entrained; hence, "rampart craters" should characterize the mare-like ridged plains rather than water-filled substrates. Fifth, radial facies indicate enhanced explosive expansion and hence the most (rather than the least) volatile-rich targets (or have been extensively modified). Sixth, anomalously long ejecta run-out distances can be created by autosuspension that feeds the vortex or flow with energy or gas (e.g., near-surface volatiles entrained by basal ejecta flow). Ninth, the development of late-stage ejecta-entrained vortices will not be significantly affected by the surrounding disturbed atmosphere (heated) since such blast effects rapidly equilibrate in the tenuous Martian atmosphere and do not drastically affect the results (8).

The above list of predictions and observations challenge some models of ejecta emplacement imposing only water. Nevertheless, the presence of volatiles can be recognized, whether in post-emplacement flow of water-lubricated near-rim ejecta or in enhanced run-out through autosuspension. Ironically, the critical importance of fine-grained lithologies may reflect enhanced weathering conditions (including fluvially transported sediments) during the Noachian and Hesperian and the role of climate-controlled processes (e.g., polar sinks for dust, obliquity changes, and polar wandering). Such considerations will not resolve the debate about Martian cratering. It simply challenges interpretations and assumptions to look further than the translating the term "fluid-

ized" into "water-entrained".

Oblique Impacts: Until relatively recently, full three-dimensional models of hypervelocity impacts have not been possible. As a result, important clues about the impact process have been gleaned from laboratory experiments compared with the planetary cratering record. Advances in computing power now has not only allowed more widespread use of 3-D codes (e.g., 9) but also enabled new diagnostics in the laboratory. These parallel advances will permit unprecedented opportunities to validate the codes and to test extrapolations to large scales, whether directly from laboratory experiments or comparisons with the codes. The oblique impact process represents one of the most challenging of these tests.

Oblique impacts map time into space. During vertical impacts, rapid changes in the transfer of energy and momentum from impactor to target are generally lost or overprinted by each successive stage of formation. Oblique impacts, however, expose this transfer along the initial trajectory. Laboratory experiments have long documented the overall change in crater dimensions and ejecta distributions (10), but new studies are providing other possible strategies for identifying the initial trajectory. First, direct measurements of far-field pressures reveal that oblique impacts cannot be simply modeled using point-source assumption (11). These measurements are clearly captured in asymmetries, timing, and nature of failure in three dimensions. Such laboratory measurements are also captured in recent computational models (9). Second, three dimensional particle image velocimetry (3D-PIV) is capturing the evolving flow field expressed by ejecta leaving the crater (12, 13). The enigmatic oblong crater shape perpendicular to the trajectory for modestly oblique impacts is now recognized in the ejecta flow field in addition to failure patterns in strength-controlled craters. Third, high-speed imaging and novel experimental designs are capturing the contact and failure pattern of the projectile.

Applying such laboratory experiments to planetary-scale phenomena and processes cannot be made without analytical or computational modeling. For example, the crater/projectile dimension ratio for cratering in sand for hypervelocity experiments is 50:1. But this ratio for large-scale (100 km) craters approach 15:1. Because oblique impacts reduce the peak pressure in the target, this ratio decreases still further to 8:1. Consequently, large-scale cratering more closely resembles strength-controlled laboratory impacts in terms of the relative dimensions of the crater and impactor. This also means that the transition from the region controlled by the transfer of momentum and energy becomes a significant fraction of the crater at large scales. Hence, observational evidence of the trajectory becomes more evident as well.

Observational evidence for impact trajectory (e.g., 15, 16) includes asymmetries in shock effects expressed by erasure/survival of pre-impact structural control, crater shape in plain view (whether oblong perpendicular to or along the trajectory), uprange offset of the central peak, breached central ring downrange, and downrange ricochet effects. Not all craters will exhibit such features. In addition to changes in expression with scale, impactor density and velocity also will play a role. For example, very high-velocity oblique impacts (>40km/s) will increase the crater/projectile ratio and partition more energy to melting and vaporization. Target topography (relative to the scale of the impactor) also can be shown to radically modify early-stage coupling processes. Consequently, statistical studies of crater morphologies may not reveal the key signatures. Such an approach is similar to including a failed experiment in laboratory impacts.

References: [1] Barlow, N., (1994) *JGR 99,* 10,927-10,935. [2] Head, J. W. III *et al.* (1999) Science 286, 2134-2137. [3] Schultz, P. H. (1979) *JGR 84,* 7669-7687. [4] Schultz, P. H. (1992) *JGR 97,* 11,623-11,662. [5] Barnouin-Jha, O. and Schultz, P. H. (1996) *JGR 101,* 21,099-21,115. [6] Barnouin-Jha, O. and Schultz, P. H. (1999) *JGR 104,* 27,105-27,116. [7] Barnouin-Jha, O. and Schultz, P. H. (1999) *JGR 104,* 27,117-27,132. [8] Barnouin-Jha, O. and Schultz, P. H. (1998) *JGR 104,* 27,105-27,116. [9] Pierazzo, E. and Melosh, H. J. (1999) *Earth Planet. Sci. Letts. 165,* 163-176. [10] Gault, D. E. and Wedekind, J. (1978) *Proc. Lunar Planet. Sci. 3rd,* 3843-3875. [11] Dahl, J. and Schultz, P. H. (2001) *Int. Jrnl. Impact Eng. 26,* 145-155. [12] Schultz, P. H., Heineck, J. T., and Anderson, J. L. B. (2000) *Lunar and Planet. Sci. XXXI,* Abst. #1902. [13] Anderson, J. A., Schultz, P. H., and Heineck, J. T. (2000) *Lunar and Planet. Sci. XXXI,* Abst. #1749. [14] Anderson, J. A.., Schultz, P. H. and Heineck, J. T. (2002, this volume). [15] Schultz, P. H. and Anderson, R. A. (1996) *Geol. Soc. Sp. Paper 302,* 397-417. [16] Sugita, S. and Schultz, P. H. (2002) *Icarus 155,* 265-284.

EXCAVATION FLOW AND CENTRAL PEAK RINGS: IS THERE A CONNECTION? V. L. Sharpton[1] and B. O. Dressler[2], [1]Geophysical Institute, University of Alaska Fairbanks, 903 Koyukuk Drive, Fairbanks, AK 99775 (buck.sharpton@gi.alaska.edu); 2 Lunar and Planetary Institute, 3600 Bay Area Blvd, Houston, TX 77058.

Introduction: To approximate the conditions associated with the excavation stage of the impact process, many numerical simulations rely on some form of the Z-model [1-5], where the radial velocity of particles below the ground surface is given by:

$$u_R = \alpha(t)/R^Z$$

and R is the radial distance from the flow origin, α is a strength parameter, and Z determines the velocity change with radial distance. While inherited from studies of explosion cratering [1-3], the Z-model has been shown to provide a first order approximation of excavation flow in simple craters as long as some appropriate effective depth of Z-model flow (EDOZ) is provided. EDOZ is usually assumed to be equivalent to one projectile diameter [e.g., 1,2,4]. The most-often applied form of this model is the steady-flow version where α, Z (~3) and EDOZ are assumed to be time constants [e.g. 1,2,5,6]. This practice, however, seems to be based on convenience rather than on sound theoretical grounds as (1) the steady flow assumption allows the flow field to be explicitly evaluated at all times [2] but (2) violates conservation of energy [1]. Furthermore, studies of laboratory-scale impacts [4,5] indicate a time-dependence to the Z-model parameters. Despite these limitations, the Z-model's ability to provide qualitative insights into the dominant spatial features of the early-time impact flow field has been emphasized [1-3]. While this may be true for laboratory scale craters and even simple craters on planetary surfaces, observations from a well-studied terrestrial complex crater indicate that neither excavation flow nor the shape of the excavation cavity are well approximated by the Z-model.

Haughton Crater. The ~24 km diameter Haughton impact crater is located at 75º 22´ N; 89º 41´ W on the western portion of Devon Island in the Canadian Arctic [7,8]. The geological map shown in Fig. 1 is derived from previous studies [9,10] with modifications resulting from our 1997 field expedition. These observations, combined with the results of reflection seismic studies [11] provide useful constraints on the target and how it was affected by the impact event. Here, we use these data to evaluate models of the size and shape of the excavation cavity generated during the formation of Haughton crater and show that these characteristics cannot be reconciled with the constant-flow Z-model. Our analysis suggests that the poorly organized peak ring at this crater reflects radial inflections in the original excavation crater prior to its uplift during late-stage modification.

The target is a nearly flat-lying sequence of Paleozoic platform rocks, ~1.8 km thick, overlying high-grade crystalline basement. The platform sequence consists of the following units [9]: **1**. The Allen Bay Fm. (OSA) limestone and dolomites, ~450 m thick. This unit forms the present surface around the crater and is found to within ~4.5 km of the center. **2**. The Cornwallis Group (OCTI) shales and carbonates with a combined thickness of ~110 m. OCTI crops out along the walls of steep valleys to the northeast of the crater. **3**. The Bay Fiord Fm. (OCB) carbonates and gypsum, ~330 m thick. Large exposures of OCB occur within 5-7 km of the crater center, as well as in valley floors as close as 8 km east of the crater center. **4**. The Eleanor River Fm. (OE) chert-bearing carbonates, ~400 m thick. Inliers of OE, representing the central uplift, occur between 0.7 and 4.8 km from crater center. The closest authochthonous OE outcrops occur ~16.5 km from the crater center. **5**. Undifferentiated Lower Ordovician-Cambrian (OCU) shale, sandstone, dolomite, and conglomerates, ~420 m thick. No parautochthonous units of OCU have been discovered within the crater; however, near the center abun-

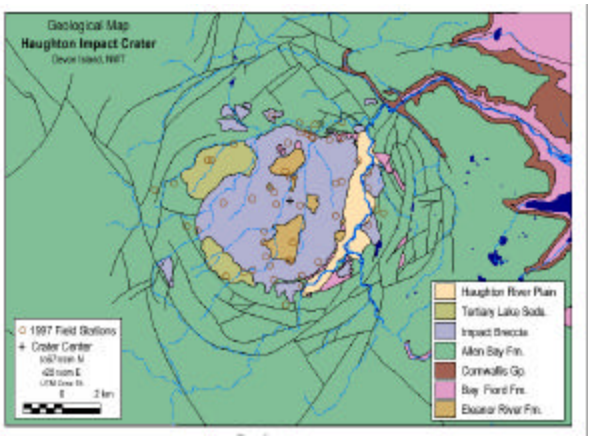

Figure 1

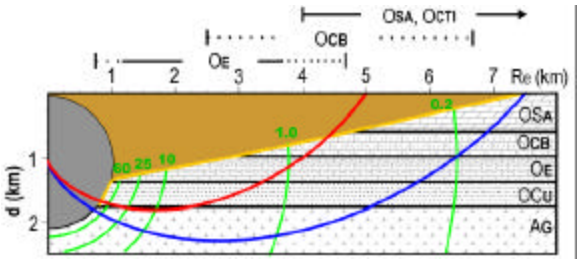

Figure 2. OCTI (not shown) is located between OSA and OCB. Shock pressures after [12].

dant highly shocked blocks of sandstone probably represent the OCU Blanley Bay Fm. Authochthonous exposures have been mapped 32 km east of crater center.

Excavation Depth and Central Uplift. Filling the shallow central basin (radius of ~5 km), the allogenic impact breccia forms a nearly continuous unit that ranges from ~10 m to over 100 m in thickness. Breccia outliers also exist beyond this deposit, with the farthest mapped deposit located ~7.8 km southeast of center. The matrix and clasts of this breccia were derived primarily from the platform rocks; however, clasts of partially melted, highly shocked, and weakly shocked clasts of Archaean high-grade metamorphic rocks (AG, Fig. 2) prove that the excavation cavity penetrated into the subjacent crystalline basement. Modal analysis [9] indicates ~10-15% of the breccia clasts are derived from the crystalline basement. Extending ~1 km from the crater center are large and extensively shatter-coned outcrops of OE (with minor OCB; Figs. 1 and 2) that form a discontinuous ring of uplifted but otherwise coherent target rocks. As their structural heights exceed the basal height of the Tertiary lake beds that filled the crater shortly after it formed, these OE exposures represent a true topographic, albeit incipient, peak ring.

Reconstructing the Excavation Crater. The excavated diameter De=2Re has been estimated at 10 km based on the incoherent zone in reflection seismic data [11]. Redeker and Stöffler [10] prefer De=15 km, based on shock isobar constraints from the Kieffer and Simonds [12] model and the need to excavate crystalline rocks. Fig. 2 shows the half-space shape of the Z=2.71 model for both the 10-km *(red line*) and 15-km *(blue line*) excavation craters predicted for Haughton crater.

Discussion. When assessed against the geological constraints provided by outcrops of parautochthonous target rocks, substantial problems with these models become evident: **1**. The Re=5 model predicts excavation completely through OE to a distance of ~3.3 km; Re=7.5 removes OE to a distance of nearly 6 km. Both therefore fail to account for the central uplift (OE derived from beneath the excavation crater) that is observed within 1.2 km of the center. **2**. Similarly, the models predict that OCB would be completely removed within 4 km (Re=5) or 6.8 km (Re=7.5) yet outcrops occur within 3 km of center and are abundant within a radius of 5 km. **3**. The Re=5 model does not account for the proportion of crystalline rock clasts observed in the allogenic breccia [10].

Conclusions. The geological constraints at Haughton crater are not compatible with a constant Z excavation flow field regardless of the choice of Re. Observations presented here constrain the zone of deep excavation to be less than 1 km from center. The *yellow line*, Fig. 2 indicates the maximum depth to the excavation crater boundary permitted by geological constraints. The resulting shape is characterized by a localized near-center zone of deep excavation – from which the crystalline rocks originate – flanked by a broad zone of shallow excavation at least 4-5 times the width of the central zone. Off-axis, deep excavation, and thus a Z-model-type of excavation flow are not incompatible with the Haughton crater observations *if and only if* Z is a strong function of time. High-Z flow (deep, near-center excavation, steep ejection angles) would occur during the earliest excavation stage and as ejection proceeded, Z, excavation depth, and ejection angle would decay.

At Haughton, the uplifted outcrops form the cusp separating two distinct sub-domains in the excavation crater: the broad outer zone of shallow excavation and the narrow, centrally located zone of deep excavation. Consequently this peak ring seems to represent a fundamental structural inflection in the base of the excavation crater that was subsequently uplifted during late-stage modification.

It is not clear whether the excavation-crater model for peak ring formation can be extended to all central peak rings, or even to those in other craters formed in layered targets. Similar excavation geometries, however, have been reported at several other complex craters with central rings [e.g. 13,14] in layered targets where such reconstructions are possible.

References: [1] Maxwell, D. E. (1977) *Impact and Explosion Cratering*, 1003-1008. [2] Croft, S. K. (1985) *Proc. Lunar Planet. Sci. Conf.* 11th, 2347-2378. [3] Orphal et al., (1977) *Impact and Explosion Cratering*, 907-917. [4] Austin et al. (1981) *Multi-ring Basins*, 197-205. [5] Austin *et al*. (1980) *Proc. Lunar Planet. Sci. Conf. 11th*, 2325-2345. [6] Collins, G. S. (2002) *Icarus 157*, 24-33. [7] Asphaug, E. and Melosh, H. J. (1993) *Icarus 101*, 144-164. [7] Frisch, T. and Thorsteinsson, R. (1978) *Artic Institute Journal* **3**1, 108-124. [8] Robertson, P. B. and Mason, G. D. (1975) *Nature 255*, 393-394. [9] Thorsteinsson, R. and Mayr, U. (1987) *Geol. Survey Can. Mem. 411*, 182 pp. [10] Redeker H.-J. and Stöffler, D. (1988) *Meteoritics 23*, 185-196. [11] Bischoff, L. and Oskierski, W. (1988) *Meteoritics 23*, 209-220. [12] Kieffer, S. W. and Simonds, C. H. (1980) *Reviews of Geophysics and Space Physics* 18, 143-181. [13] Brennan, R. L. *et al*. (1975) *WY Geol Assoc. Earth Sci. Bull. 8*, 41 pp. [14] Milton, D. J. *et al*. (1972) *Science 175*, 1199-1207.

MECHANISMS OF IN SITU ROCK DISPLACEMENT DURING HYPERVELOCITY IMPACT: FIELD AND MICROSCOPIC OBSERVATIONS J.G. Spray, Planetary and Space Science Centre, University of New Brunswick, Fredericton, NB E3B 5A3, Canada. jgs@unb.ca

Introduction: The nature of rock deformation due to hypervelocity impact is discussed, especially with regard to the larger terrestrial structures (e.g., Sudbury, Vredefort, Manicouagan). Based on field observations and thin section microscopy, evidence is presented for two end-members of rock response to extreme strain rates: (1) bulk deformation, due to pervasive fracture generation and ensuing micro-displacement with melting; (2) localized large-displacement faulting, accompanied by friction melt generation (pseudotachylytes). There is no evidence for bulk "fluidization" at the thin section scale, except where bulk melting has occurred during impact melt sheet generation, wherein truly fluid (igneous) rocks are formed.

S- and E-type fracture-fault systems: Bulk deformation in footwall rocks beneath the Sudbury Igneous Complex (melt sheet) is limited to a zone some 10-15 km beyond the contact with overlying melt. Fracture-microfault systems are typically a few mm thick and are akin to shock veins in meteorites. These have been referred to as S-type pseudotachylytes [1]. They may contain high-pressure polymorphs. Melting is probably due to a combination of shock and microslip. In this proximal footwall zone at Sudbury, there are 10-20 pervasive S-type veins per cubic meter, with the frequency decreasing progressively away from the melt sheet.

Localized, large-displacement faulting can be related to concentric and radial structures that appear to be formed during the modification stage of the cratering process. These post-date the shock wave and are primarily driven by gravitational forces and possible rebound effects. Movement on the concentric systems commonly occurs after movement on the radials. Movement on the concentric faults is typically significantly greater than that realized on the radial fracture-fault systems. Large displacement, single slip faults have been referred to as superfaults when displacement is >100 m in one event [2]. Under superfaulting conditions, thick (1-1000 m) friction melt (pseudotachylyte) bodies may result. These may be responsible for the rings seen in multiring impact basins on the moon and other planets. The thickest pseudotachylytes are formed when these faults undergo displacements of several kilometers in one slip event. Superfaults generate terraces in the larger impact structures. This class of pseudotachylyte has been referred to as E-type [1]. E-type pseudotachylytes are formed in the same way as endogenic fault-related pseudotachylytes, though displacements due to impact can be many orders of magnitude greater than those realized during regular faulting (the latter typically resulting in cm-wide pseudotachylyte veins).

Central uplifts: While S- and E-type pseudotachylytes have been documented with regard to melt sheet footwall occurrences, there are very few references made to them with regard to the internal structure of central uplifts. Central uplift mechanics remains poorly understood. How is it possible for vast volumes of rock to move, supposedly downwards (during compression) many kilometres, and then back up many kilometres (on decompression), and probably within seconds or minutes? In fact, there is little hard evidence that transient cavities are pushed downwards during compression and excavation (i.e., in a gross plastic/elastic manner). In so, cannot rebound be attributed merely to pressure release at a free surface? The internal structure of central uplifts has not been studied in any real systematic detail in the field. Work on smaller impact structures, such as Decaturville [3] reveals a crude concentric piston-like form, with the deepest level rocks being exposed in the centre of the uplift and successively higher level rocks being exposed around this core. The uplift is thus not chaotic, although each concentric zone appears to comprise blocks of coherent rock in a fragmental matrix (breccia) that has been well mixed. Preliminary work thus indicates that some uplifts are similar to telescopic hydraulic rams in their cylinder-within-cylinder structure. Whether the contacts between "cylinders" are sharp (i.e., fault bounded) or gradual (fluid like), is not yet clear.

References: [1] Spray, J.G. (1998) *Spec. Pub. Geol. Soc. London* 140, 195-204. [2] Spray, J.G. (1997). *Geology* 25, 579-582. [3] Nickerson, G.A.J. (2002) Unpublished MSc thesis, University of New Brunswick, Canada, 127 p.

TOWARD A COMPLETE MEASUREMENT OF THE THERMODYNAMIC STATE OF AN IMPACT-INDUCED VAPOR CLOUD. Seiji Sugita[1], Keiko Hamano[1], Toshihiko Kadono[2], Peter H. Schultz[3], and Takafumi Matsui[1], [1]University of Tokyo (7-3-1 Hongo, Bunkyo-ku, Tokyo, JAPAN, sugita@eps.s.u-tokyo.ac.jp), [2]IFREE, JAMSTEC (2-15 Natushima-cho, Yokosuka, Kanagawa, JAPAN), [3]Brown University (Providence, RI 02912, USA).

Introduction: Vaporization phenomena induced by hypervelocity impacts play an important role in the origin and evolution of Earth and other planets. There have been extensive research efforts made for understanding this process. However, the equation of state (EOS) and chemical reaction within high-pressure and high-temperature conditions of impact vapor are yet highly uncertain [e.g., 1, 2]. This is primarily owing to the lack of experimental data on impact vapor cloud. Here we discuss newly developed spectroscopic methods to determine the thermodynamic state of impact-induced vapor very accurately.

Thermodynamic State of Impact Vapor: Among the four fundamental thermodynamic quantities (temperature T, pressure p, entropy s, and density ρ), two of them are necessary to designate the thermodynamic state of an equilibrium system. If the system has a multiple components and is ionized, both chemical composition x and ionization ratio ϕ are also needed to describe the system. The spectroscopic methods we have developed can obtain sufficient thermodynamic quantities to designate uniquely the thermodynamic state of a system.

Spectroscopic Method: The emission spectra of rapidly evolving impact vapor clouds have to be taken with high resolution in both time and wavelength. This had been extremely difficult until an intensified charge-coupled device (ICCD) arrays were introduced. They are capable of taking a thousand of different wavelengths of light at once with an extremely short exposure time (up to ~10 ns). This permits obtaining high-quality emission spectra of impact vapor clouds.

Temperature T. When a high-resolution spectrum is obtained, the intensities of emission lines are measured to generate a Boltzmann diagram (Fig.1), which shows the logarithm of emission intensities I normalized by transition probability A, statistical weight g, and photonic energy $h\nu$ as a function of the upper energy level E of the transition divided by Boltzmann constant. The inverse of the slope in a Boltzmann diagram gives the temperature T of the measured vapor [e.g., 3,4,5].

Chemical Composition x. Once a Boltzmann diagram is made, one can also obtain the chemical composition. The vertical intercept of a fit line gives the logarithm of the number of ground state atoms, which is approximately the total number of atoms in vapor clouds generated in a laboratory [3,4,5]. Then the difference in the intercepts of two different atoms (Cu and Ca in Fig.1) in a Boltzmann diagram gives the ratio of the two atoms: atomic composition x.

Ionization ratio ϕ. Some atoms exhibit very strong ion emission lines. When these ion lines are treated as a different atom and a Boltzmann diagram is made, the number ratio of ionized to neutral atoms is obtained. This gives the ionization ratio ϕ [3,4].

Density ρ. The density of high-temperature plasma can be estimated by spectral line profile of emission lines. Some atoms such as hydrogen exhibit a large line width due to Lorentz broadening, which is proportional to 2/3rd power of electron density [3]. Laboratory experiments show that such Lorentz broadening can be observed with high enough accuracy to obtain a reliable value of electron density. The electron density can be converted to the bulk vapor density ρ using ionization ratio ϕ and chemical composition x [6].

Application to Planetary-Scale Impacts: The above methods have a wide variety of application in hypervelocity impact study. An immediate application is to study the EOS of highly compressed impact vapor, which may be highly different from an ideal gas. When the thermodynamic state of an impact vapor cloud is determined, the chemical reaction processes within the vapor cloud can be estimated much more easily. Such knowledge will help understand the problem of sulfur oxides in the K/T impact vapor cloud [7]. Furthermore, a quantitative comparison between impact- and laser-induced vapor clouds can be done with these methods. It will widen the range of the application of laser-simulated "impact vapor clouds" greatly [2,8]

References: [1] Stevenson, D.J. (1987) *Ann. Rev. Earth Planet. Sci*., *15*, 271. [2] Muhkin et al. (1989) *Nature, 340*, 46 [3] Griem, H.R. (1964) *Plasma Spectroscopy*. [4] Sugita S. et al. (1998) *JGR, 103,* 19,427. [5] Sugita S. et al., *JGR, 104*, 30,825. [6] Hamano, K. et al. (2002) *Proc. 35th Lunar Planet. Symp.* 174. [7] Ohno, S. et al. (2002) *EPSL,* submitted. [8] Kadono, T. et al. (2002) *GRL*, in press.

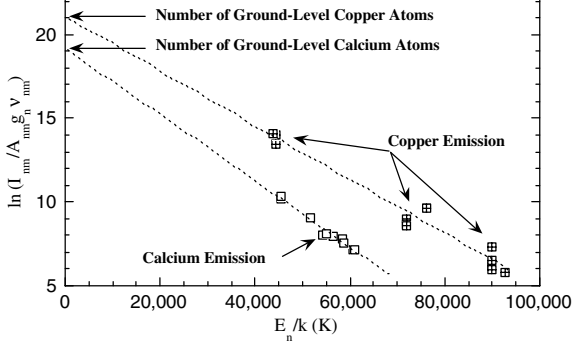

Fig. 1. Boltzmann diagram of an impact vapor cloud. The vapor cloud is induced by copper projectile impacting dolomite target. The copper and calcium emissions represent the projectile and target components, respectively.

COOLING OF THE KÄRDLA IMPACT CRATER: I. THE MINERAL PARASEQUENCE OBSERVATIONS. E. Versh[1], A. Jõeleht[2], K. Kirsimäe[3] and J. Plado[4], [1,2,3,4]Institute of Geology, University of Tartu, Vanemuise 46, Tartu 51014, Estonia ([1]desty@ut.ee, [2]ajoeleht@ut.ee, [3]arps@ut.ee, [4]jplado@ut.ee).

Introduction: Kinetic energy released to the target by a meteorite impact results in the heating-to-melting and vaporization of the projectile and target rocks, which then start to cool to the ambient conditions. In dry environments (e.g. Moon) the heat loss occurs mainly by conduction and radiation transfer. If the water is present at the crater site as on Earth and supposedly on Mars, then the cooling can include also convective heat transfer by hydrothermal circulation systems. Evidences of impact-induced hydrothermal activity have been found at many terrestrial craters [1], and it is suggested for extraterrestrial craters as well [2]. Cooling and development of such impact-induced hydrothermal systems can be recognized by the means of (1) mineralogical/fluid inclusion studies, and (2) by impact and geothermal modeling.

In this and following paper (see Jõeleht et al., in this volume) we report a complex geological observation and modeling study of post-impact cooling of a medium-to-small scale impact crater of Kärdla, Hiiumaa Island, Estonia. The Kärdla crater is 4 km in diameter and ~540 m deep with a central uplift exceeding 100 m height above crater floor. It formed in a shallow (<100 m deep) epicontinental Ordovician sea ~455 Ma ago into a target composed of thin siliciclastic and carbonate sedimentary sequence covering crystalline basement [3]. In this first part of our contribution we present the results of mineralogical, fluid inclusion and stable isotope studies.

Mineral parasequence: The crater-fill sequence at Kärdla crater hosts up to 400 m thick allochthonous and autochthonous breccias that have undergone water-rock interaction. A complex clay-feldspar-carbonate(Fe-oxyhydrate) assemblage characterizes the post-impact hydrothermal mineralization. The most intensive alteration is found in breccias and shattered basement around and above the central uplift. The results of homogenization temperature measurements of quartz fluid inclusions in allochthonous breccia encompass a wide range from 110 to 440°C, with the maximum between 150 and 300°C [4] (Fig). This temperature range is in agreement with the chloritic minerals formation temperatures of 150-325°C. However, the mineral paragenesis suggests that the main phase of chloritization was preceded by earlier cryptocrystalline K-feldspar formation, whereas the second generation of euhedral K-feldspar inside fractures and voids precipitated after the chlorite, probably at temperatures of 200-100°C. Dolomite-calcite and sulfides/Fe-oxyhydrates (hematite and goethite) reflect the final stages of cooling when temperature reached ambient conditions. Calculated fluid equilibrium temperatures for carbonates indicate that those fluid temperatures were below 100ºC (in the range of 75-35°C).

Initial temperatures: Studies of hydrothermal mineral assemblages and fluid inclusions provide information about the post-impact temperatures and enables the mapping of thermal aureole. However, studies of mineral parageneses lack in information on the life times of these hydrothermal systems and the cooling time is not assessed by this approach. Heat and fluid transfer simulations can resolve that question. However, this needs the initial post-impact temperature distribution to be known. Mineral geothermometry results suggest maximum initial temperatures at least 150-300°C in the central part of the Kärdla crater. The same is suggested by PDF studies in shocked quartz, which refer to the maximum shock pressures during the impact event in a range of 20-35 GPa [5]. The distribution of the most frequent fluid inclusion homogenization temperatures suggests also approximately the same range (Fig). However, the high temperature inclusions on homogenization temperature graph suggest trapping temperatures as high as 350-450°C.

Comparison with the preliminary results of the hydrocode modeling of impact (Jõeleht et al., in this volume) shows that the initial temperatures remaining in the rocks estimated by geothermometry are significantly higher than the model predictions using Tillotson equation of state, but are in general agreement when ANEOS is used. The details of modeling problems are discussed in part II by Jõeleht et al. (see this volume).

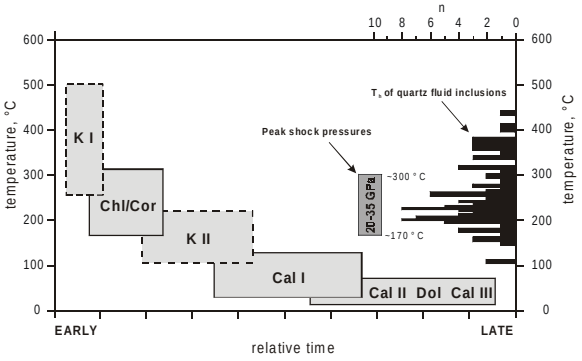

Fig. Post-impact hydrothermal mineralization parasequence at Kärdla crater. Shock pressures (20-35 GPa) from [5] and histogram of aqueous (H2O-NaCl) quartz fluid-inclusion homogenization temperatures (T_h) from [4] are shown at the RH side. K - K-feldspar, Chl/Cor - chlorite/corrensite, Cal - calcite, Dol - dolomite; I, II, III - 1st, 2nd and 3rd generation. Formation temperatures for chlorite-corrensite and carbonate minerals are estimated form geothermometry and stable isotope composition, respectively. Positions of K-feldspar I and II fields are tentatively assumed from paragenetic relationships with chloritic and carbonate minerals.

References: [1] Naumov M.V. (2002) *Impacts in Precambrian Shields*, pp. 117-171. [2] Newsom H.E. (1980) *Icarus*, 44, 207-216. [3] Puura V. and Suuroja K. (1992) *Tectonophysics*, 216, pp. 143-156. [4] Kirsimäe K. et al. (2002) *Meteoritics & Planet. Sci.*, 37, 449-457. [5] Puura et al. (submitted) *Meteoritics & Planet. Sci.*